

# Stereo Hand-Object Reconstruction for Human-to-Robot Handover

Yik Lung Pang, Alessio Xompero, Changjae Oh, Andrea Cavallaro

**Abstract**—Jointly estimating hand and object shape ensures the success of the robot grasp in human-to-robot handovers. However, relying on hand-crafted prior knowledge about the geometric structure of the object fails when generalising to unseen objects, and depth sensors fail to detect transparent objects such as drinking glasses. In this work, we propose a stereo-based method for hand-object reconstruction that combines single-view reconstructions probabilistically to form a coherent stereo reconstruction. We learn 3D shape priors from a large synthetic hand-object dataset to ensure that our method is generalisable, and use RGB inputs instead of depth as RGB can better capture transparent objects. We show that our method achieves a lower object Chamfer distance compared to existing RGB based hand-object reconstruction methods on single view and stereo settings. We process the reconstructed hand-object shape with a projection-based outlier removal step and use the output to guide a human-to-robot handover pipeline with wide-baseline stereo RGB cameras. Our hand-object reconstruction enables a robot to successfully receive a diverse range of household objects from the human.

## I. INTRODUCTION

As humans and robots work together more closely [1], exchanging objects is one of the essential skills to enable smooth collaboration between humans and robots. In particular, human-to-robot handover is the exchange of objects between a human giver and a robot receiver [2]. In this highly interactive scenario, hand-object shape reconstruction is an essential task as the object shape informs the robot about how to grasp the object, while the hand shape allows the robot to avoid potentially dangerous contact with the human.

Visual modalities, including RGB and depth, are used in hand-object shape reconstruction for human-to-robot handover. Previous works [3]–[7] used depth sensors to capture the pointcloud of the scene and applied segmentation models to extract the pointcloud of the hand and object. Depth sensors can capture opaque objects but not transparent objects in the scene [8], causing the robot to fail to handover objects such as glasses. To accommodate transparent objects, some works have attempted to perform human-to-robot handovers with wide-baseline stereo RGB cameras [9]. However, these works can only handle container-like objects as they assume that the object is upright and rotationally symmetric.

We consider the scenario where a person hands over various objects to a robot and the robot aims to grasp the object successfully while avoiding the human, and place the object at a predefined delivery location (Fig. 1). Container-like objects, such as drinking cups and glasses, can be empty

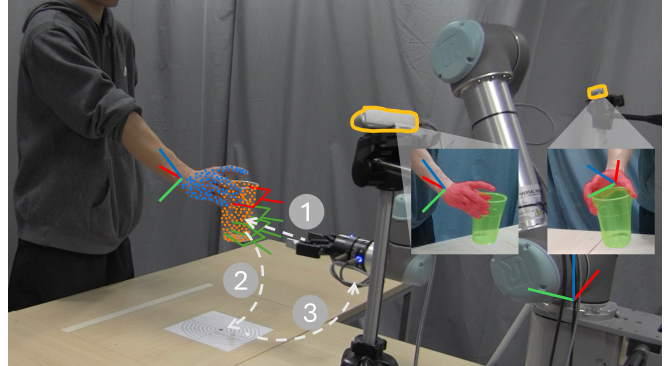


Fig. 1: We reconstruct the hand-object pointcloud from stereo RGB input for human-to-robot handover. (1) A safe grasp is selected for the handover and the robot moves in to grasp the object. (2) The object is delivered to a target location on the table. (3) The robot returns to its starting position.

or filled with content. The presence of content can alter the appearance of transparent containers which affects the performance of depth-based methods. Unlike depth cameras, RGB cameras can capture the appearance of generic objects, including transparent objects. Moreover, capturing stereo views instead of a single view can help tackle the issue of occlusion by increasing the visible area of the hand and object to the model [10].

We propose StereoHO<sup>1</sup>, a hand-object reconstruction model for wide-baseline stereo inputs. Our method quantifies the uncertainty of single-view predictions, and take the uncertainty into account when forming the stereo reconstruction. For each local 3D patch, we predict the shape as a probability distribution over a set of learned discrete shape embeddings. A high variance represents an uncertain prediction that may be caused by issues such as occlusion. Predictions from the left and right views are then combined via element-wise multiplication and decoded jointly to form the stereo reconstruction. We train our model entirely on synthetic 3D hand-object data [11] with a large amount of objects and without specific assumptions about the object’s geometry to ensure its generalisation ability.

We then present the first human-to-robot handover method that jointly reconstructs hand and object shape from stereo RGB inputs. We apply our proposed reconstruction method on wide-baseline stereo cameras and track the hand’s movement over time. To ensure multi-view consistency, the reconstructed pointcloud is projected back to the left and right

Yik Lung Pang, Alessio Xompero, and Changjae Oh are with Centre for Intelligent Sensing, Queen Mary University of London, UK {y.l.pang, a.xompero, c.oh}@qmul.ac.uk

Andrea Cavallaro is with Idiap Research Institute and École Polytechnique Fédérale de Lausanne, Switzerland a.cavallaro@idiap.ch

<sup>1</sup>Code and videos of the experiments available at <https://qm-ipalab.github.io/StereoHO/>

camera views and points outside of the hand and object segmentation masks are removed.

Experiments show that our hand-object reconstruction method outperforms previous methods in single-view and stereo settings for object reconstruction, while remaining competitive for hand reconstruction in terms of Chamfer distance. When integrated into a human-to-robot handover pipeline, our method can successfully handover objects of diverse shapes and appearances, including filled/empty transparent containers, boxes and thin objects like CDs.

## II. RELATED WORK

### A. Perception for human-to-robot handover

Recent works in human-to-robot handover [3]–[7], [9], [12] focused on markerless settings as it is more applicable to in-the-wild human-to-robot interactions. Human grasps were classified into different types based on a human grasp taxonomy to select the corresponding predefined safe robot grasp direction and enable the robot to receive the object [3]. This approach limits the grasp types that the robot can handle as the high degree of hand articulation implies that there is a continuous distribution of many possible ways for a human to grasp an object. Moreover, to handle a diverse set of objects, the object shape should be considered.

Later works improved the perception by capturing the shape of the hand and the object [4]–[7], [9], [12], and used existing grasp estimation methods to predict possible grasps on the object shape. Grasps that would cause a collision between the robot and the human are removed for safety. A two-stage system was proposed to perform human-to-robot handovers of everyday objects [4]. The human and the object are first segmented from the input RGB image. The depth image is then lifted into a pointcloud and the background is removed using the segmentation masks. Finally, an imaginary plane is added in the grasping direction to approximate the task as a top-down grasp estimation problem using GG-CNN [13]. To enable more natural handovers [5], 6-DoF grasps are used to perform the handover to allow more freedom in the robot’s movement.

Pointcloud is a common representation for the shape of the human hand and the object in existing methods for human-to-robot handovers [4]–[7], as pointclouds can be directly obtained from a depth sensor and grasp estimation methods rely on this representation [13], [14]. Although pointclouds retrieved from a depth sensor is accurate enough for human-to-robot handover, the shape retrieved is dependent on the view direction. The object shape is often incomplete due to occlusions, affecting the grasping performance. Depth sensors cannot reliably detect transparent and reflective objects, causing failure in the grasp estimation. Depth restoration overcomes this issue and completes the pointcloud of transparent objects [15]. However, a depth camera is still required which is not as commonly available as RGB cameras.

Other methods use stereo RGB images as input to reconstruct the shape of the object [9], [12]. The shape of containers, such as drinking glasses and cups, was reconstructed from stereo RGB images by assuming a rotationally

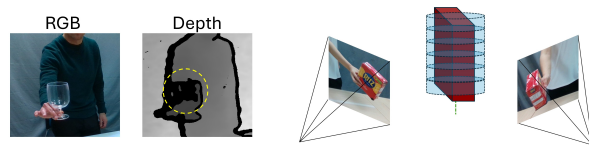


Fig. 2: Depth-based sensing fails on transparent objects (left), while relying on shape priors is not generalisable (right).

symmetric geometry and exploiting the predicted segmentation masks of the object [16]. This enables human-to-robot handover by grasping at the centroid of the object [9]. Safety of the human can be considered by estimating the 3D hand keypoints [12]. Robot grasps are sampled along the vertical axis of the object and grasp points that are too close to the hand keypoints are removed. However, these methods do not estimate 6-DoF grasps and thus limit the naturalness of the robot movement as the object must maintain an upright orientation during the handover. The assumption on the object shape can also be easily invalidated by non-container objects, causing failure in the object shape estimation. Furthermore, estimating the shape of both the hand and the object provides more information for the human’s safety.

### B. Hand-object reconstruction from RGB images

Joint hand-object reconstruction from RGB images in an interaction scenario is challenging due to severe mutual occlusions between the hand and the object [11]. Large hand-object interaction datasets, both synthetic and collected in real environments [11], [17], [18], have helped improve the reconstruction quality. Existing methods can be grouped into single-view and multi-view, and multi-view methods can be further split into dense and sparse. Single-view reconstruction methods [11], [19]–[21] learn 3D shape priors from hand-object datasets, but remains challenging as the method has to complete the shape of the unobserved parts of the object. Multi-view methods [10], [22]–[25] overcome the problems of occlusion and unobserved object parts by increasing the number of input views. In particular, dense multi-view methods [22]–[25] can produce high quality reconstructions but require a large number of input views and computationally expensive optimisation strategies, limiting the applicability in reactive scenarios such as human-to-robot handovers. Sparse multi-view methods [10] balances the reconstruction quality of dense methods with the speed of single-view methods. However, training only on synthetic data can affect the model’s ability to generalise to real world scenarios (sim-to-real gap) [10].

## III. PROPOSED METHOD

In this section, we introduce StereoHO for stereo hand-object reconstruction. We detail how we tackle the sim-to-real gap when training on synthetic data, highlight how our method combines single-view predictions for stereo reconstruction, and present our human-to-robot handover pipeline.

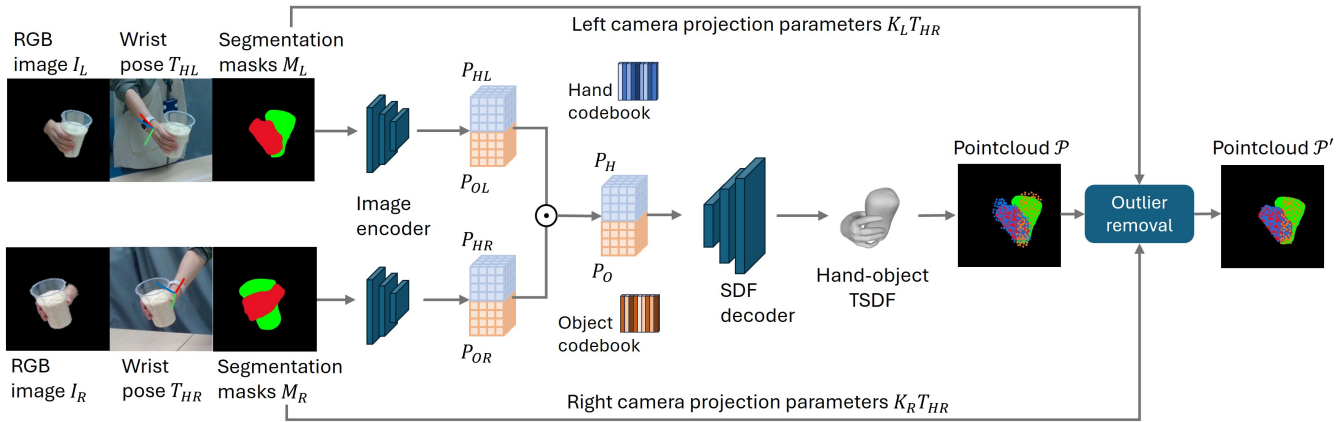


Fig. 3: Our proposed hand-object reconstruction method with two cropped images from a wide-baseline stereo camera. StereoHO first performs shape estimation from each view independently to obtain the predicted probability distributions,  $P_L = \{P_{HL}, P_{OL}\}$  and  $P_R = \{P_{HR}, P_{OR}\}$ , over the shape codebooks. The stereo-based probability distribution  $P = \{P_H, P_O\}$  is computed by element-wise multiplication of  $P_L$  and  $P_R$ . The trained SDF decoder transforms the stereo prediction into the hand-object TSDF. Surface points, sampled as a pointcloud  $\mathcal{P}$  from the TSDF, are projected into each view using the predicted camera projection parameters. We use the segmentation masks to remove the outliers to obtain the final pointcloud  $\mathcal{P}'$ . KEYS –  $K$ : intrinsics calibration parameters,  $L$ : left view,  $R$ : right view;  $H$ : hand,  $O$ : object.

#### A. Stereo-based RGB hand-object reconstruction

Given stereo RGB images  $I$  cropped and centred on the hand, wrist poses  $T_H$  and hand-object segmentation masks  $M \in \{M_H, M_O\}$  in each view, our method predicts the pointcloud  $\mathcal{P} \in \{\mathcal{P}_H, \mathcal{P}_O\}$  representing the surface of the hand and object jointly over both views. We task the network to predict the signed distance fields (SDF) of the hand and object as an intermediate step. Compared to pointclouds, SDF represents smooth continuous surfaces and is easier to learn [26]. We train our model only on synthetic data. As segmentation masks are domain-invariant, and to facilitate sim-to-real transfer, we include hand and object segmentation masks as input to the model. The object segmentation mask allows our model to avoid erroneously including background clutter in the reconstructed shape.

To combine individual predictions for a coherent stereo reconstruction, the model should consider and weigh their uncertainty. For example, uncertainty should be higher for areas that are occluded and lower for areas that are clearly visible. To achieve this, we treat the hand-object shape reconstruction as a local shape classification task based on a learned discrete shape codebook. The output is a predicted probability distribution  $P$  over the discrete codes where the variance of the distribution represents the uncertainty of the prediction. We learn this discrete shape codebook by training a 3D autoencoder with vector quantization to obtain quantized shape embeddings on a synthetic hand-object dataset [11]. We train an image encoder to predict the probability distribution of shape codes for each local 3D patch from the individual input views and the learned shape codebook. The predicted probability distributions from each view are combined into a single prediction via element-wise multiplication. We obtain the most likely shape code at each local 3D patch and decode the global shape jointly to ensure a coherent hand-object shape.

#### B. Learning discrete 3D shape embeddings

To learn the 3D shape embeddings, we train a 3D P-VQ-VAE autoencoder [27] to encode the hand and object truncated signed distance field (TSDF) independently. We extract the TSDF of each training sample and use 3D convolution layers to encode the shape of local patches. We also use the vector quantization process to obtain a codebook of 3D shape embeddings. The SDF decoder applies 3D convolution layers to the 3D shape embeddings jointly to retrieve the SDF values. We train the autoencoder using the following loss function,

$$\mathcal{L}_{ae} = \|s - \hat{s}\| + \|sg[z_e] - e\|_2^2 + \beta \|z_e - sg[e]\|_2^2, \quad (1)$$

where  $s$  and  $\hat{s}$  are the ground truth and predicted SDF values,  $e$  is the vector quantized shape embedding,  $z_e$  is the shape embedding output by the encoder before vector quantization,  $sg$  is the stop gradient operator, and  $\beta$  is the hyper-parameter controlling the scale of the commitment loss.

#### C. From single-view predictions to stereo reconstruction

We reconstruct the hand and object shape from each view by predicting the learned 3D shape embeddings for each local patch. We use the trained encoder to extract the 3D shape embeddings for each training sample and the index corresponding to the codebook entry. We treat shape estimation as a classification task by predicting the codebook index corresponding to the shape embedding at each local 3D patch. We use the following weighted cross-entropy loss,

$$\mathcal{L}_{ce}(p, p_{gt}) = - \sum_c^C w_c \cdot p_{gt}(c) \cdot \log p(c), \quad (2)$$

where  $p$  and  $p_{gt}$  are the predicted and ground truth probability for index  $c$ ,  $C$  is the codebook size and  $w_c$  is the weight for the index  $c$ .

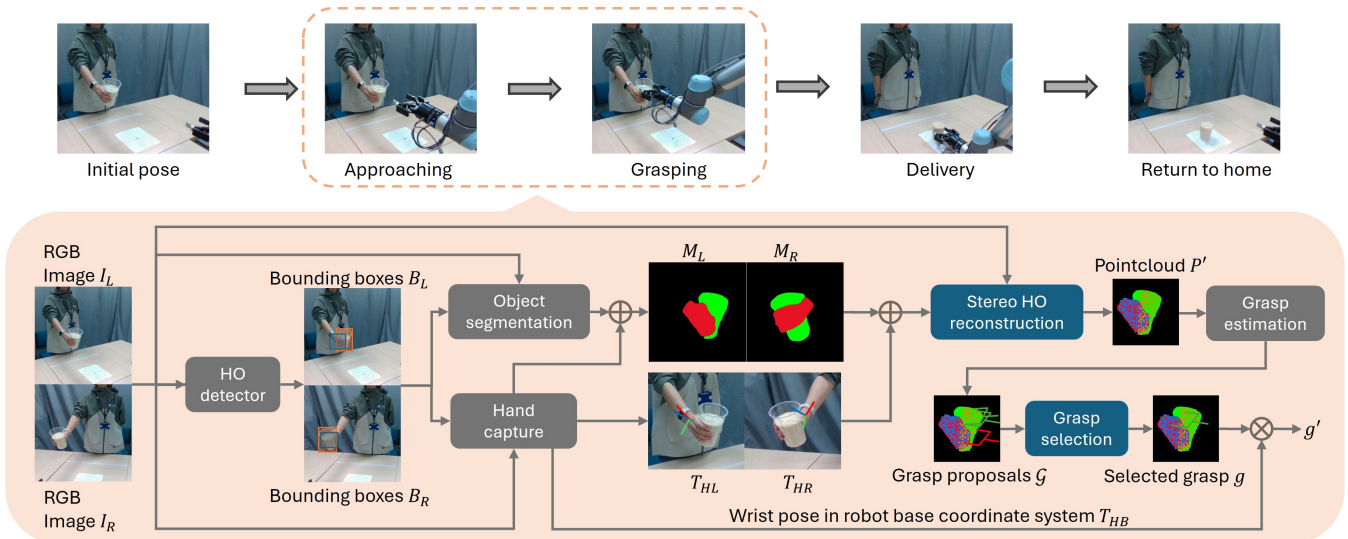


Fig. 4: Our proposed robot control pipeline for human-to-robot handover (modules from other works are in grey). We first perform hand-object detection to obtain bounding boxes  $B$ . Hand-object segmentation masks  $M$  and wrist poses  $T_H$  are estimated on the image cropped around the hand. We combine the outputs from the preprocessing steps for stereo hand-object reconstruction to obtain pointcloud  $\mathcal{P}'$ . Grasp estimation is performed on the reconstructed shape and transformed at each timestep using the wrist poses  $T_{HB}$ . The wrist pose in robot coordinate space  $T_{HB} = T_{WB} * T_{HW}$  is calculated using the world to robot base transform  $T_{WB}$  obtained using the hand-eye calibration process [28].

We build a canonical 3D representation by constructing a 3D grid centred on the hand wrist and retrieve the corresponding image embedding for each local patch by projecting the 3D position to 2D image space using the wrist pose  $T_{HL}$  and  $T_{HR}$ . The resulting 3D representation is processed with 3D convolution layers and the probability distribution  $P_L$  and  $P_R$  over codebook size  $C$  is predicted per local patch for the left and right views, respectively.

To obtain the overall stereo prediction, we multiply the predicted probability distributions from the left and right views:  $P = P_L \cdot P_R$ . To obtain the pointcloud of the hand and object  $\mathcal{P}_H$  and  $\mathcal{P}_O$ , we extract TSDF values in a grid using the trained SDF decoder and keep the points within a threshold SDF value of 1 cm to the surface.

#### D. Handover with stereo hand-object reconstruction

We integrate StereoHO into a pipeline for human-to-robot handovers. We use two cameras on either side of the robot to maximise the visible area of the hand and object.

To perform stereo hand-object reconstruction, we first obtain the necessary inputs from the RGB image. For each view, a hand-object detector estimates the bounding boxes of both the hand and the object. The object bounding box is used as a prompt for object segmentation, whereas we use the bounding box of the hand to crop the image around the hand. The cropped image is used as input to a hand capture module that predicts the shape of the hand and the pose of the wrist. We remove the background from the cropped image by using the object segmentation mask and the segmentation mask of the hand, extracted as a silhouette from the shape of the hand.

We use the cropped image, the pose of the wrist, and the segmentation masks to reconstruct the pointclouds of the

hand and the object using StereoHO. We ensure multi-view consistency by reprojecting the predicted hand and object pointcloud  $\mathcal{P}_H$  and  $\mathcal{P}_O$  back to the RGB images and keep only the points that are within the segmentation masks  $M_H$  and  $M_O$ , respectively. Since the reconstruction can change at each timestep, it can significantly affect the grasp estimation quality. Therefore, we only update the predicted pointclouds if there is an improvement in reconstruction quality. We compute the Intersection over Union (IoU) of the convex hull of the pointclouds with the segmentation masks, respectively, and only accept the updated reconstruction if the IoU is greater than the previous best IoU.

#### E. Object receiving and delivery

Given the pointclouds predicted by our hand-object reconstruction model, we estimate a set of 6-DoF grasps,  $\mathcal{G} = \{g_n \in SE(3)\}_{n=1}^N$ , on the object pointcloud  $\mathcal{P}'_O$ . The predicted grasps  $\mathcal{G}$  are in the hand wrist coordinate frame and is transformed using the predicted wrist pose  $T_{HB}$  to the robot base coordinate frame. To ensure the safety of the human, we filter out any grasps that are colliding with the hand point cloud  $\mathcal{P}'_H$ .

The robot control selects the grasp  $g$  closest to the current gripper 6D pose at every timestep. We define a standoff position 15 cm away from the grasp point in the direction of the grasp. Once the robot reaches the standoff position, the robot enters a close-loop grasping stage and closes its fingers when the gripper reaches the selected grasp.

After the grasp  $g$  is executed, the robot retracts for 15 cm back to the standoff position. The robot then moves to a predefined delivery location and opens the gripper fingers to place the object on the table. Finally, the robot returns to its home position ready for the next handover.

## F. Implementation details

For hand-object reconstruction, we set  $w_c = 0.25$  for the index  $c$  corresponding to empty space and  $w_c = 0.75$  for the rest of the codebook as the majority of the space surrounding the hand and object is empty. We use ResNet-18 [29] pre-trained on ImageNet [30] as our image encoder. During the handover, we use hand-object detector [31] to obtain hand-object bounding boxes, Fast Segment Anything [32] for object segmentation, FrankMocap [33] for hand capture, and 6-DoF GraspNet [14] for grasp estimation.

## IV. VALIDATION

### A. Datasets

We train our hand-object reconstruction model on the ObMan [11] dataset and test on the DexYCB [17] dataset. ObMan is a fully simulated hand-object dataset using the MANO hand model [34] with ShapeNet [35] objects. The object classes include bottles, bowls, cans, jars, knives, cellphones, cameras and remote controls. DexYCB is a hand-object dataset captured using an 8 camera setup in a lab environment. 20 objects from the YCB-Video dataset [36] were used including cans, boxes and various everyday objects.

### B. Handover setup

We follow an existing benchmarking protocol [9] that includes a setup of the robotic and perception systems, and 288 handover configurations to execute. The setup includes a 6-DoF Universal Robots UR5 robotic arm, equipped with a Robotiq 2F-85 2-finger gripper for grasping the object, and two Intel Realsense D435 cameras mounted on tripods on either side of the robotic arm pointing at the workspace of the robot which is a wooden table with the target delivery location marked on the surface. The protocol configurations are executed by 4 participants who hand over 3 disposable cups and 1 plastic wine glass, either empty or filled with rice, using 3 different grasp types and at 3 handover locations (72 configurations for each participant). To assess generalisation to different novel objects, each participant execute another 15 configurations for 5 objects at the 3 different handover locations using 1 grasp type (a total of 60 configurations). These additional objects vary in size, topology, and appearance (e.g., reflectiveness), and include a tea box, a cracker box, a tape, a screwdriver, and a CD (see Fig. 5).

We compare our human-to-robot handover method with the stereo RGB method [12] designed specifically for container-like objects<sup>2</sup>. For [12], the objects start on the table at the centre of the delivery target and participants are asked to pick up the object and give it to the robot. The object on the table is first detected using Mask R-CNN [37] pretrained on the COCO dataset [38]. The shape is then estimated using LoDE [16]. The mask is tracked with SiamMask [39] in subsequent frames and the 3D object centroid is triangulated from the 2D centroid in the left and

<sup>2</sup>Approval for this research was obtained from the Queen Mary Ethics of Research Committee Ref:QMERC20.525 on 19/10/2021. Consent from each human subject was obtained prior to the experiments.



Fig. 5: Objects used for the handover experiments: three cups and a drinking glass, empty or filled with rice, from an existing benchmarking protocol [9] (left image), and additional household objects (right image), such as tea box (O1), cracker box (O2), tape (O3), screwdriver (O4), and CD (O5), to assess generalisation.

right view. The container is assumed to be upright at all times throughout the handover process and hand keypoints are estimated using OpenPose [40] per frame. Grasp points are generated along the height of the container and grasp points that are close to the hand keypoints in height are removed. The robot starts moving once the object is lifted off the table. For our method, since we assume the human is already holding the object, we ask the participants to hold the object behind a starting line indicated by tape on the wooden table. The robot starts moving towards the object once the human moves the object beyond the starting line.

### C. Performance measures

We use chamfer distance to evaluate hand and object reconstructions. The chamfer distance between the ground-truth and predicted point sets  $S$  and  $\hat{S}$  is

$$d_{CD}(S, \hat{S}) = \sum_{x \in S} \min_{y \in \hat{S}} \|x - y\|_2 + \sum_{y \in \hat{S}} \min_{x \in S} \|x - y\|_2 \quad (3)$$

To evaluate the performance of the human-to-robot handover methods, we use three measures from the CORSMAL benchmark [9], including delivery location ( $\delta$ ), efficiency ( $\gamma$ ), and delivered mass ( $\mu$ ), and two other measures, including grasping success ( $G$ ) and delivery success ( $D$ ).

For *delivery location*, we measure the distance from the center of the base of the delivered container to a predefined delivery location on the table as  $d$  in mm,

$$\delta = \begin{cases} 1 - \frac{d}{\rho}, & \text{if } d < \rho, \\ 0, & \text{otherwise.} \end{cases} \quad (4)$$

We set  $\rho = 500$  mm as the maximum accepted distance.

We quantify the *efficiency* of each handover configuration as the amount of time  $t$  required from the moment the robot starts moving towards the object to the moment the object is delivered on the table,

$$\gamma = \begin{cases} 1 - \frac{\max(t, \eta) - \eta}{\tau - \eta}, & \text{if } t < \tau, \\ 0, & \text{otherwise.} \end{cases} \quad (5)$$

The less time required, the more efficient the method is, and the higher the efficiency score  $\gamma$ . The score is scaled based on the expected minimum time required  $\eta = 1,000$  ms and the maximum time required  $\tau = 15,000$  ms.

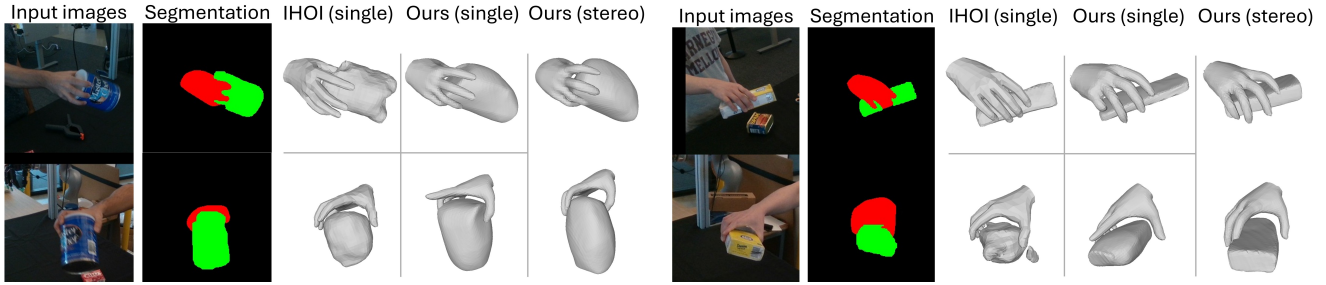


Fig. 6: Comparison of single view and stereo hand object reconstructions on DexYCB [17]. For the single-view setting, each reconstruction corresponds to the image on the same row. For the stereo setting, the same reconstruction is shown from two viewpoints. Our method yields less noisy reconstruction by introducing segmentation masks as input. In the stereo setting, our method improves both the hand and object reconstructions by combining the predictions from individual views.

For the *delivered mass*, when the container is filled with rice, the robot is expected to deliver the container to the delivery location without spilling the content. We quantify the performance of the delivery based on the difference between the total mass  $m$  of the filled container delivered and the total mass  $\hat{m}$  of the filled container before the handover,

$$\mu = \begin{cases} 1 - \frac{|m - \hat{m}|}{\hat{m}}, & \text{if } |m - \hat{m}| < \hat{m}, \\ 0, & \text{otherwise,} \end{cases} \quad (6)$$

We measure *grasping success* as the configurations where the robot is able to grasp and hold the object without dropping it after retracting.

We quantify *delivery success* of each configuration as the successful placement of the container on the table within the maximum delivery distance  $\rho$  with no content spilled:

$$D = \begin{cases} 1, & \text{if } d < \rho \text{ and } |m - \hat{m}| = 0, \\ 0, & \text{otherwise.} \end{cases} \quad (7)$$

Note that since the additional objects are not containers, we do not report on the delivered mass  $\mu$  and we remove the condition  $|m - \hat{m}| = 0$  from the delivery success  $D$ .

#### D. Hand-object reconstruction from RGB

Since our reconstruction method combines individual single-view predictions from the left and right views to form the stereo prediction, we evaluate our method in both single-view and stereo settings.

We compare StereoHO with IHOI [19] in the single-view setting and with SVHO [10] in the stereo setting. IHOI is an SDF-based method that predicts the shape of the object conditioned on the pose of the hand, and is trained end-to-end. SVHO is a sparse multi-view method that reconstructs hand-object shape and can be easily adapted to use only two views. For a fair comparison, we train our method, IHOI, and SVHO, only on the synthetic data of ObMan, and evaluate the methods using DexYCB [17]. We select the two views closest to the stereo views of our setup and compare the reconstruction quality (see Fig. 6). For the single-view setting, we aggregate results from both the left and right views. We separate the objects in the testing set into seen and unseen categories based on the similarity in 3D shape between the training and testing objects.

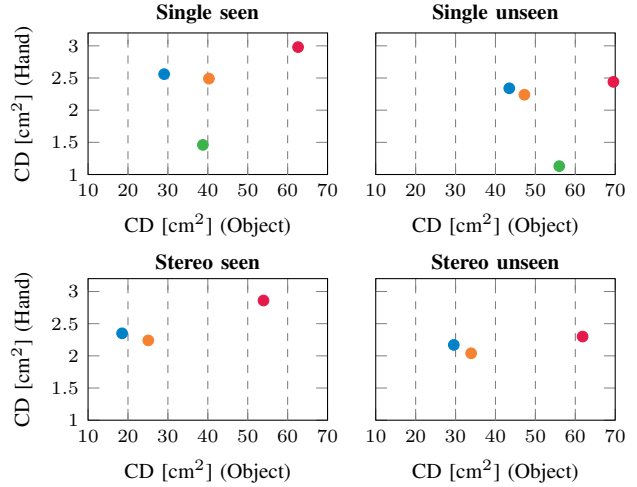


Fig. 7: Single-view and stereo hand-object reconstruction errors on DexYCB [17]. Best results on the bottom-left corner. Legend: CD: chamfer distance, ■ SVHO [10], ■ IHOI [19], ■ Ours (no segmentation mask), ■ Ours. IHOI, as a single-view reconstruction method, is not evaluated in stereo setting.

In the single-view setting (Fig. 7), our method outperforms IHOI on object reconstruction by  $9.71 \text{ cm}^2$  and  $12.52 \text{ cm}^2$ , while slightly underperforming on hand reconstruction by  $1.10 \text{ cm}^2$  and  $1.21 \text{ cm}^2$  in the seen and unseen categories, respectively. In the stereo setting, our method outperforms SVHO on object reconstruction by  $35.43 \text{ cm}^2$  and  $32.27 \text{ cm}^2$ , while performing slightly better on the hand reconstruction by  $0.51 \text{ cm}^2$  and  $0.13 \text{ cm}^2$  in the seen and unseen categories, respectively. Compared with a version of our method without segmentation masks as input, our method improves the object reconstruction while sacrificing a small amount of performance in hand reconstruction. This also results in less noisy reconstructions as shown in Fig. 6 when comparing with IHOI in the single-view setting.

#### E. Human-to-robot handovers

We first evaluate the methods with the objects from the CORSMAL benchmark (Tab. I). Both [12] and our method achieve over 75% grasping success and 65% delivery success. This shows that assuming a cylindrical prior and a mostly upright pose throughout the task is reasonable when

TABLE I: Comparing handover performance between [12] which performs grasping with fixed rotation and our method which performs 6-DoF grasping with rotation. We validate on (Left) container-like objects from the CORSMAL benchmark with and without rice, and (Right) additional household objects. Our method is able to handover container-like objects and additional household objects, while [12] cannot handle the additional household objects as the perception module does not recognize non-container objects and hence cannot perform the handover.

Score	Ref.	Container-like objects					Grasp types			Filling		Household objects					
		All	C1	C2	C3	C4	TOP	MID	BOT	E	FR	All	O1	O2	O3	O4	O5
Delivery location $\delta$	[12]	0.45	<b>0.52</b>	0.58	0.33	0.38	<b>0.47</b>	0.35	0.53	0.40	<b>0.51</b>	–	–	–	–	–	–
	Ours	<b>0.48</b>	0.26	<b>0.65</b>	<b>0.59</b>	<b>0.42</b>	0.45	<b>0.45</b>	<b>0.55</b>	<b>0.47</b>	0.49	0.18	0.18	0.11	0.06	0.25	0.31
Efficiency $\gamma$	[12]	<b>0.29</b>	<b>0.31</b>	<b>0.35</b>	<b>0.26</b>	<b>0.25</b>	<b>0.31</b>	<b>0.29</b>	<b>0.29</b>	<b>0.79</b>	<b>0.78</b>	–	–	–	–	–	–
	Ours	0.10	0.12	0.09	0.10	0.09	0.10	0.10	0.10	0.10	0.10	0.10	0.09	0.07	0.07	0.14	0.13
Delivered mass $\mu$	[12]	<b>0.78</b>	<b>0.77</b>	0.81	0.77	<b>0.78</b>	<b>0.81</b>	<b>0.81</b>	0.84	<b>0.79</b>	<b>0.78</b>	–	–	–	–	–	–
	Ours	0.74	0.53	<b>0.87</b>	<b>0.84</b>	0.73	0.66	0.69	<b>0.88</b>	0.76	0.72	–	–	–	–	–	–
Grasping success $G$	[12]	<b>0.79</b>	<b>0.77</b>	0.81	0.79	<b>0.80</b>	<b>0.82</b>	<b>0.72</b>	0.84	<b>0.79</b>	<b>0.80</b>	–	–	–	–	–	–
	Ours	0.75	0.55	<b>0.88</b>	<b>0.84</b>	0.73	0.66	0.69	<b>0.89</b>	0.76	0.74	0.70	0.50	0.66	0.75	0.75	0.83
Delivery success $D$	[12]	<b>0.67</b>	<b>0.73</b>	0.77	0.50	<b>0.68</b>	<b>0.72</b>	0.53	0.76	0.61	<b>0.73</b>	–	–	–	–	–	–
	Ours	0.66	0.36	<b>0.86</b>	<b>0.84</b>	0.59	0.63	<b>0.58</b>	<b>0.78</b>	<b>0.69</b>	0.63	0.58	0.41	0.58	0.50	0.58	0.83

Best scores are highlighted in **bold** for each column and each performance measure. KEY – TOP: top, MID: middle, BOT: bottom, E: empty, FR: full rice, Ref.: reference. C1: small white cup, C2: red cup, C3: beer cup, C4: wine glass, O1: tea box, O2: cracker box, O3: tape, O4: screwdriver, O5: CD.

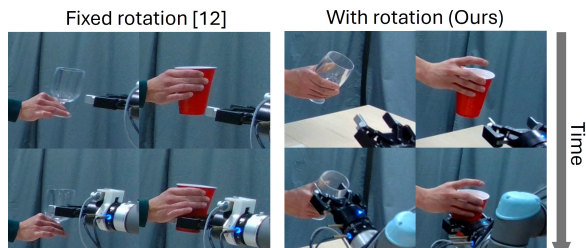


Fig. 8: Our method allows the robot to perform grasping with 6-DoF, resulting in more natural handovers, compared to [12] that performs grasping with fixed rotations.

handing over cups and drinking glasses [12]. However, [12] performs grasping with a fixed rotation, forcing the subjects to adapt to the robot’s gripper pose (Fig. 8). On the contrary, the 6-DoF grasping of our method allows the subject to be more natural, but at the cost of being computationally more expensive and achieving a lower efficiency score (0.10).

Results per object show that our method can successfully handover transparent objects with minimal degradation in performance. The grasping and delivery scores for beer cup (transparent object) only differ by 0.04 and 0.02, respectively, compared to those of red cup (opaque object). Our method also performs better on larger objects and detects the object already handheld. Smaller objects are hard to detect for our method due to occlusions from the hand and background clutter from the clothes of the participants. On the contrary, [12] performs better on smaller objects because the detection starts when the object is unoccluded and on the table with a uniform background. Results by grasp type show that our method performs best when objects are handed over with the bottom grasp. Note that this grasp type is more common in the training set of our reconstruction model. The middle grasp leaves the least amount of space on the container for the robot to grasp, decreasing the performance of [12].

Tab. I also shows that our method achieved 70% grasping success and 58% delivery success when handing the ad-

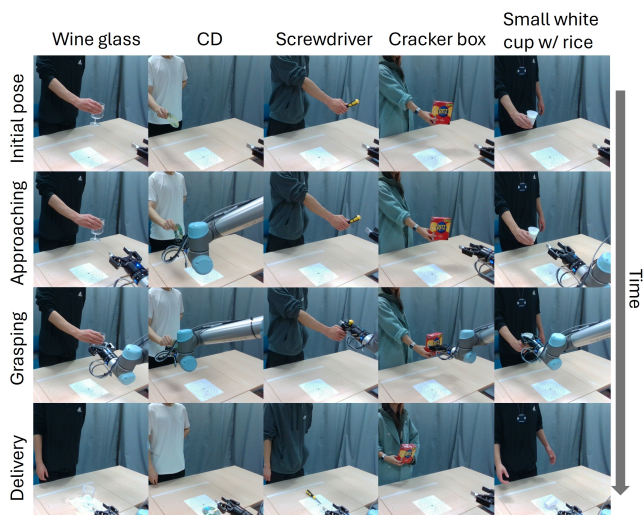


Fig. 9: Example handovers. Each column shows a single configuration from initialisation to object delivery.

ditional household objects over to the robot, whereas [12] cannot detect them as they are not present in the COCO dataset [38]. Specifically, our method can successfully receive objects with challenging shape, such as thin objects (the screwdriver), hollow objects (the tape), and reflective objects (the CD). Failures occur when the reconstruction of the object shape is inaccurate. For example, the robot often mistakenly try to grasp the cracker box from the wider side, which is not possible for the width of the gripper (see Fig. 9). Another mode of failure occurs when the robot loses track of the hand due to occlusions by the object or the robot arm.

## V. CONCLUSION

In this paper, we tackled the task of joint hand-object reconstruction using wide baseline stereo RGB cameras. We showed that our reconstruction method outperforms existing methods in single-view and stereo settings. Moreover, we showed that our method enables a robot to receive empty

and filled containers, and can generalize to other household objects. Future work includes improving the speed of handovers and the quality of hand-object reconstructions.

### ACKNOWLEDGMENT

This project made use of time on Tier 2 HPC facility JADE2, funded by EPSRC (EP/T022205/1).

### REFERENCES

- [1] S. Kumar, C. Savur, and F. Sahin, "Survey of human-robot collaboration in industrial settings: Awareness, intelligence, and compliance," *IEEE Trans. Systems, Man, and Cybernetics: Systems*, vol. 51, no. 1, pp. 280–297, 2020.
- [2] V. Ortenzi, A. Cosgun, T. Pardi, W. P. Chan, E. Croft, and D. Kulić, "Object handovers: a review for robotics," *IEEE Trans. Robotics*, vol. 37, no. 6, pp. 1855–1873, 2021.
- [3] W. Yang, C. Paxton, M. Cakmak, and D. Fox, "Human grasp classification for reactive human-to-robot handovers," in *IEEE Int. Conf. Intell. Robot Syst.*, 2020, pp. 11 123–11 130.
- [4] P. Rosenberger, A. Cosgun, R. Newbury, J. Kwan, V. Ortenzi, P. Corke, and M. Grafinger, "Object-independent human-to-robot handovers using real time robotic vision," *IEEE Robotics Autom. Lett.*, vol. 6, no. 1, pp. 17–23, 2020.
- [5] W. Yang, C. Paxton, A. Mousavian, Y.-W. Chao, M. Cakmak, and D. Fox, "Reactive human-to-robot handovers of arbitrary objects," in *IEEE Int. Conf. Robotics Autom.*, 2021.
- [6] W. Yang, B. Sundaralingam, C. Paxton, I. Akinola, Y.-W. Chao, M. Cakmak, and D. Fox, "Model predictive control for fluid human-to-robot handovers," in *IEEE Int. Conf. Robotics Autom.*, 2022.
- [7] L. Wang, Y. Xiang, W. Yang, A. Mousavian, and D. Fox, "Goal-auxiliary actor-critic for 6D robotic grasping with point clouds," in *Conf. Robot Learning*, 2022.
- [8] S. Sajjan, M. Moore, M. Pan, G. Nagaraja, J. Lee, A. Zeng, and S. Song, "ClearGrasp: 3D shape estimation of transparent objects for manipulation," in *IEEE Int. Conf. Robotics Autom.*, 2020.
- [9] R. Sanchez-Matilla, K. Chatzilygeroudis, A. Modas, N. F. Duarte, A. Xompero, P. Frossard, A. Billard, and A. Cavallaro, "Benchmark for human-to-robot handovers of unseen containers with unknown filling," *IEEE Robotics Autom. Lett.*, vol. 5, no. 2, pp. 1642–1649, 2020.
- [10] Y. L. Pang, C. Oh, and A. Cavallaro, "Sparse multi-view hand-object reconstruction for unseen environments," in *Conf. Comput. Vis. Pattern Recognit. Workshops*, 2024.
- [11] Y. Hasson, G. Varol, D. Tzionas, I. Kalevtykh, M. J. Black, I. Laptev, and C. Schmid, "Learning joint reconstruction of hands and manipulated objects," in *Conf. Comput. Vis. Pattern Recognit.*, 2019.
- [12] Y. L. Pang, A. Xompero, C. Oh, and A. Cavallaro, "Towards safe human-to-robot handovers of unknown containers," in *IEEE Int. Conf. Robot & Human Interactive Communication*, 2021.
- [13] D. Morrison, P. Corke, and J. Leitner, "Closing the loop for robotic grasping: A real-time, generative grasp synthesis approach," in *Robotics: Science and Syst.*, 2018.
- [14] A. Mousavian, C. Eppner, and D. Fox, "6-DoF GraspNet: Variational grasp generation for object manipulation," in *Int. Conf. Comput. Vis.*, 2019.
- [15] R. Yu, H. Yu, H. Yan, Z. Song, S. Li, and W. Ding, "Depth restoration of hand-held transparent objects for human-to-robot handover," 2024, arXiv:2408.14997v2 [cs.RO].
- [16] A. Xompero, R. Sanchez-Matilla, A. Modas, P. Frossard, and A. Cavallaro, "Multi-view shape estimation of transparent containers," in *Proc. IEEE Int. Conf. Acoustics, Speech Signal Process.*, 2020.
- [17] Y.-W. Chao, W. Yang, Y. Xiang, P. Molchanov, A. Handa, J. Tremblay, Y. S. Narang, K. Van Wyk, U. Iqbal, S. Birchfield, J. Kautz, and D. Fox, "DexYCB: A benchmark for capturing hand grasping of objects," in *Conf. Comput. Vis. Pattern Recognit.*, 2021.
- [18] L. Yang, K. Li, X. Zhan, F. Wu, A. Xu, L. Liu, and C. Lu, "Oakink: A large-scale knowledge repository for understanding hand-object interaction," in *Conf. Comput. Vis. Pattern Recognit.*, 2022.
- [19] Y. Ye, A. Gupta, and S. Tulsiani, "What's in your hands? 3D reconstruction of generic objects in hands," in *Conf. Comput. Vis. Pattern Recognit.*, 2022.
- [20] Z. Chen, S. Chen, C. Schmid, and I. Laptev, "gSDF: Geometry-driven signed distance functions for 3D hand-object reconstruction," in *Conf. Comput. Vis. Pattern Recognit.*, 2023.
- [21] H. Choi, N. Chavan-Daffe, J. Yuan, V. Isler, and H. Park, "HandNeRF: Learning to reconstruct hand-object interaction scene from a single RGB image," in *IEEE Int. Conf. Robotics Autom.*, 2024.
- [22] S. Hampali, T. Hodan, L. Tran, L. Ma, C. Keskin, and V. Lepetit, "In-hand 3D object scanning from an RGB sequence," in *Conf. Comput. Vis. Pattern Recognit.*, 2023.
- [23] A. Swamy, V. Leroy, P. Weinzaepfel, F. Baradel, S. Galaoui, R. Brégier, M. Armando, J.-S. Franco, and G. Rogez, "Showme: Benchmarking object-agnostic hand-object 3D reconstruction," in *Int. Conf. Comput. Vis.*, 2023.
- [24] W. Qu, Z. Cui, Y. Zhang, C. Meng, C. Ma, X. Deng, and H. Wang, "Novel-view synthesis and pose estimation for hand-object interaction from sparse views," in *Int. Conf. Comput. Vis.*, 2023.
- [25] Y. Ye, P. Hebbbar, A. Gupta, and S. Tulsiani, "Diffusion-guided reconstruction of everyday hand-object interaction clips," in *Int. Conf. Comput. Vis.*, 2023.
- [26] Z. Chen and H. Zhang, "Learning implicit fields for generative shape modeling," in *Conf. Comput. Vis. Pattern Recognit.*, 2019.
- [27] P. Mittal, Y.-C. Cheng, M. Singh, and S. Tulsiani, "AutoSDF: Shape priors for 3D completion, reconstruction and generation," in *Conf. Comput. Vis. Pattern Recognit.*, 2022.
- [28] R. Y. Tsai and R. K. Lenz, "A new technique for fully autonomous and efficient 3D robotics hand/eye calibration," *IEEE Trans. Robotics Autom.*, vol. 5, no. 3, pp. 345–358, 1989.
- [29] K. He, X. Zhang, S. Ren, and J. Sun, "Deep residual learning for image recognition," in *Conf. Comput. Vis. Pattern Recognit.*, 2016.
- [30] J. Deng, W. Dong, R. Socher, L.-J. Li, K. Li, and L. Fei-Fei, "Imagenet: A large-scale hierarchical image database," in *Conf. Comput. Vis. Pattern Recognit.*, 2009.
- [31] D. Shan, J. Geng, M. Shu, and D. F. Fouhey, "Understanding human hands in contact at internet scale," in *Conf. Comput. Vis. Pattern Recognit.*, 2020.
- [32] X. Zhao, W. Ding, Y. An, Y. Du, T. Yu, M. Li, M. Tang, and J. Wang, "Fast segment anything," 2023, arXiv:2306.12156v1 [cs.CV].
- [33] Y. Rong, T. Shiratori, and H. Joo, "FrankMocap: A monocular 3D whole-body pose estimation system via regression and integration," in *Int. Conf. Comput. Vis. Workshops*, 2021.
- [34] J. Romero, D. Tzionas, and M. J. Black, "Embodied hands: Modeling and capturing hands and bodies together," *ACM Trans. Graph.*, vol. 36, no. 6, Nov. 2017.
- [35] A. X. Chang, T. Funkhouser, L. Guibas, P. Hanrahan, Q. Huang, Z. Li, S. Savarese, M. Savva, S. Song, H. Su, J. Xiao, L. Yi, and F. Yu, "ShapeNet: An information-rich 3D model repository," 2015, Stanford University — Princeton University — Toyota Technological Institute at Chicago, arXiv:1512.03012v1 [cs.GR].
- [36] Y. Xiang, T. Schmidt, V. Narayanan, and D. Fox, "PoseCNN: A convolutional neural network for 6D object pose estimation in cluttered scenes," in *Robotics: Science and Syst.*, 2018.
- [37] K. He, G. Gkioxari, P. Dollár, and R. B. Girshick, "Mask R-CNN," in *Int. Conf. Comput. Vis.*, 2017.
- [38] T.-Y. Lin, M. Maire, S. Belongie, J. Hays, P. Perona, D. Ramanan, P. Dollár, and C. L. Zitnick, "Microsoft COCO: Common objects in context," in *Eur. Conf. Comput. Vis.*, 2018.
- [39] Q. Wang, L. Zhang, L. Bertinetto, W. Hu, and P. Torr, "Fast online object tracking and segmentation: A unifying approach," in *Conf. Comput. Vis. Pattern Recognit.*, 2019.
- [40] T. Simon, H. Joo, I. Matthews, and Y. Sheikh, "Hand keypoint detection in single images using multiview bootstrapping," in *Conf. Comput. Vis. Pattern Recognit.*, 2017.